

Selected Paper

Synthesis of a Highly Hydrophobic Cationic Lipid and Structural and Thermodynamic Studies for Interaction with DNA

Tomoki Nishimura,[1] Takeshi Cho,[1] Andrew M. Kelley,[2] Magdalena E. Powell,[2] John S. Fossey,[3] Steven D. Bull,[2] Tony D. James,[2] Hiroyasu Masunaga,[4] Isamu Akiba,[1] and Kazuo Sakurai*[1]

[1]Department of Chemistry and Biochemistry, The University of Kitakyushu, 1-1 Hibikino, Wakamatsu-ku, Kitakyushu 808-0135

[2]Department of Chemistry, The University of Bath, Claverton Down, Bath, BA1 7AY, UK

[3]School of Chemistry, University of Birmingham, Edgbaston, Birmingham, B15 2TT, UK

[4]SPring-8 Japan Synchrotron Radiation Research Institute (JASRI), 323-3 Mihara, Mikazuki, Sayo-gun, Hyogo 679-5198

Received March 12, 2010; E-mail: sakurai@env.kitakyu-u.ac.jp

Synthetic DNA-transfection reagents can overcome safety issues raised by use of viral DNA vectors. One of these candidates is a cationic lipid that can form a supramolecular complex with DNA. We have been working in a series of aromatic diamine lipids with different tail length from C6 to C18: [*N*-(3,5-dialkylbenzyl)ethane-1,2-diamine, denoted DA] as such a lipid. The present paper describes the synthesis and the fundamental properties of DA. SAXS from DA solution showed bilayer vesicle formation, while it showed lamellar formation after the complexation with DNA. When we measured the N/P ratio (molar ratio of the amine groups (N) in DA to phosphate groups (P) in the DNA) dependence of SAXS, the lamellar peak (spacing = 5.0 nm) increased proportionally to the added DNA concentration at $N/P \geq 8$. On the other hand, in the range of $N/P < 8$, the spacing was increased to 5.5 nm and the area decreased as DNA increased. These different features between $N/P \geq 8$ and $N/P < 8$ suggest that the lamellar supramolecular structures differ according to the composition.

Complexes made from DNA and cationic lipids have attracted enormous scientific and technical interest since the early 1980s, and complexes of liposomes have become known as "lipoplexes."[1] Interactions between oppositely charged DNA and cationic lipids condense DNA into a more compact form as opposed to its highly extended conformation in solutions. This process has been thought to take place through three steps: (1) An electrostatic binding between the cationic headgroups and the negatively charged phosphate groups of DNA, (2) endothermic dehydration of the water bound to DNA, and (3) at higher lipid-to-DNA ratios, condensation results in the formation of globular structures. Considerable interest has been generated in lipoplexes since Felgner et al.[2] first found that certain complexes formed from DNA and synthetic cationic lipids could be efficient vehicles for DNA or RNA delivery into a wide variety of eukaryotic cells. After almost 20 years since the first invention, the mechanism of transfection is still not well understood, and further investigation is necessary to improve the transfection efficiency for the adaptation of lipoplexes to clinical and practical use.[1]

It is generally believed that lipoplexes can facilitate the ingestion of DNA in the endocytosis pathway and subsequently transport the DNA from endosomal to cytosol vesicles. Some studies have suggested that the lipoplex structure is the major critical factor in determining the transfection efficiency. Small-angle X-ray scattering (SAXS) studies of lipoplexes by Safinya et al.[3–7] demonstrated that lipoplexes take three predominant phases: (a) A multi-lamellar phase where DNA is intercalated into lipid bilayers ($L_\alpha{}^C$), (b) an inverted hexagonal phase with DNA encapsulated within monolayers tubes, arranged in a two-dimensional hexagonal lattice ($H_{II}{}^C$), and (c) the cationic lipids form rod-like micelles arranged in a hexagonal lattice with DNA inserted within the interstices with a honeycomb symmetry ($H_I{}^C$). It was shown that $H_{II}{}^C$ exhibited the highest transfection and its superior efficiency was attributed to the unstable nature of the encapsulated DNA and bound lipids.[7] Recently, Marty et al.[8] studied the same system as Safinya et al.[3,5] (i.e., DNA/DOTAP) with FTIR and found that there are molecular contacts between the lipid aliphatic tails and DNA. This result cannot be explained in the framework of any structure of $H_I{}^C$, $H_{II}{}^C$, and $L_\alpha{}^C$.

Independently from those studies, we reported that aromatic amine and amidine derivatives can be used as transfection reagents with better efficiency and less toxicity than commercial products.[9–11] A liposome made from an amidine derivative is now in clinical trials for protein delivery.[12] We reported that there could be another hexagonal phase where the DNA/cationic ion pairs are included inside of the cylinder and the cylinder surface is covered with the remaining unbound lipids (we denoted "hexagonally packed bilayer DNA-inclusion cylinders," i.e., $H_b{}^C$).[13] Our data showed that the aromatic amine and amidine derivatives did not take $H_{II}{}^C$ at any composition and $H_I{}^C$ gave better transfection efficiency than $H_b{}^C$. Recently, Koynova et al.[14–16] synthesized more than 20 cationic phosphatidylcholine derivatives with different tail lengths and showed that an intracellular phase transition occurs

Published on the web August 21, 2010; doi:10.1246/bcsj.20100072

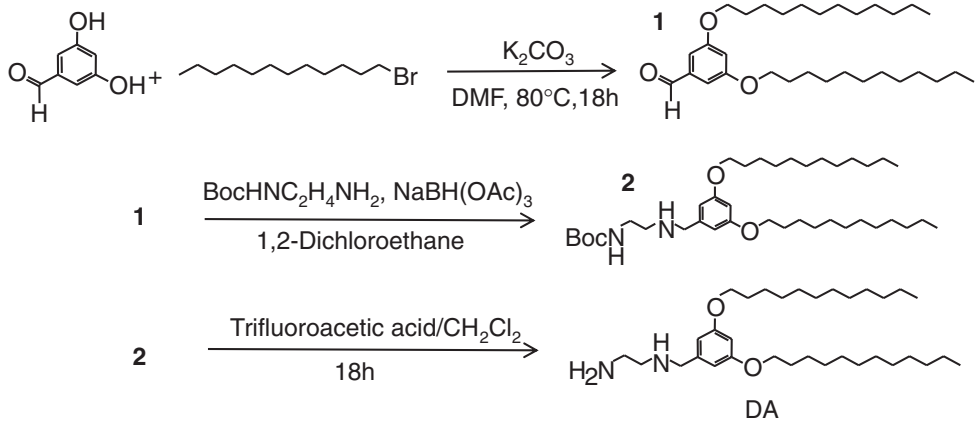

Figure 1. Synthetic scheme of the new aromatic diamine lipid for gene delivery disclosed in a preceding patent.[9]

when a certain lipoplex meets a cellular vesicle bilayers, the ability to induce this phase transition relates to the superior performance of transfection. They showed that $L_{\alpha}{}^{C}$ can give better transfection than others in the case that $L_{\alpha}{}^{C}$ can be transformed into cubic phase when it is mixed with cellular membranes. Although different cationic lipids may lead to different conclusions, it seems that the principle to relate transfection and lipoplex structures has not been established.

Isothermal titrations had previously revealed that lipoplex formation is a cooperative processes, mainly driven by an entropy increase and opposed by a relatively small endothermic enthalpy.[17–19] These workers also found a large negative heat capacity change, indicating contribution from hydrophobic interactions between the alkyl tails and counter ion release from DNA upon binding lipids. These thermodynamic studies can be interpreted by a lateral interaction of the alkyl tails: the cationic headgroups are localized at the DNA phosphates, while hydrophobic tails would be associated with each other and lay down on the DNA surface to exclude water.[17,18] This structure seems to contradict that from SAXS, where the alkyl tails stand perpendicular to the DNA surface and associate through van der Waals forces. One cause of complexity in studying lipoplexes is that most of the cationic lipids need co-lipid to enhance their biocompatibility or to form stable micelles in aqueous solutions, most importantly, to increase transfection efficiency. Generally, DOPE (dioleoylphosphatidylethanolamine) is added as well as other co-lipids such as DLPC and DOPC.

We found that *N*-(3,5-dialkylbenzyl)ethane-1,2-diamine (DA, Figure 1) derivatives themselves can form a stable vesicle in water and addition of a small amount of DOPE led to a drastic increase in transfection efficiency.[10] In order to understand the molecular mechanism for the transfection of the DA/DOPE system, we decided to take advantage of the good water-compatibility of DA to study interactions of DA vesicle and DNA. This paper presents data and analysis relating to the binding of various DAs with different tail length (C6–C18) to DNA based on several physical measurements including synchrotron SAXS and isothermal titration calorimetry.

Experimental

Synthesis of DA-Lipids. A solution of 3,5-dihydroxybenzaldehyde (0.5 g, 4.53 mmol), 1-bromododecane (2.81 g, 11.3 mmol), and K_2CO_3 (3.41 g, 22.7 mmol) was stirred at 80 °C in dry DMF (25 mL) for 18 h under an argon atmosphere. The reaction mixture was cooled to rt, water (25 mL) was added and the aqueous phase extracted with CH_2Cl_2. The product was purified by flash chromatography over silica gel using CH_2Cl_2 as eluent, **1** was obtained after evaporation of the solvent (1.83 g, 85%). ^{1}H NMR (500 MHz, $CDCl_3$): δ 9.89 (1H, s, CHO), 6.98 (2H, s, ArH), 6.70 (1H, s, ArH), 3.98 (4H, t, $J =$ 6.3 Hz, 2 × OCH_2), 1.79 (4H, q, $J = 6.9$ Hz, 2 × OCH_2CH_2), 1.48–1.42 (4H, m, 2 × OCH_2CH_2), 1.34–1.22 (44H, br s, 2 × $C_{11}H_{22}$), 0.88 (6H, t, $J = 6.5$ Hz, 2 × CH_3).

Sodium triacetoxyhydroborate (1.23 g, 5.78 mmol) was slowly added to a mixture of **1** (1.82 g, 3.85 mmol) and *N*-(*tert*-butoxycarbonyl)ethane-1,2-diamine (0.62 g, 3.85 mmol) in 1,2-dichloroethane (10 mL). The resultant solution was stirred at rt for 24 h under an argon atmosphere. The reaction was then quenched with saturated $NaHCO_3$ solution and stirred for 30 min, extracted with CH_2Cl_2, dried over $MgSO_4$, and purified by flash chromatography over silica gel using CH_2Cl_2:methanol = 9:1 as eluant. Compound **2** was obtained as a pale yellow oil after evaporation of solvent (1.29 g, 54%). ^{1}H NMR (500 MHz, $CDCl_3$): δ 6.46 (2H, s, ArH), 6.38 (1H, s, ArH), 6.06 (1H, br s, $NHCO_2$), 3.91 (4H, t, $J = 6.5$ Hz, 2 × OCH_2 and 2H, s, CH_2NHCO_2), 3.44 (2H, s, $ArCH_2$), 2.95 (2H, s, $NHCH_2CH_2NHCO_2$), 1.98 (4H, m, 2 × OCH_2CH_2), 1.45–1.41 (13H, br s, $OC(CH_3)_3$ and 2 × $OCH_2CH_2CH_2$), 1.30–1.25 (44H, br s, 2 × $C_{11}H_{22}$), 0.88 (6H, t, $J = 6.9$ Hz, 2 × CH_3).

Compound **2** (1.29 g, 2.08 mmol) was dissolved in dry CH_2Cl_2 (2 mL), then trifluoroacetic acid (18 mL) was added at rt and then stirred for 7 h. The resultant solution was poured into saturated $NaHCO_3$ solution (100 mL). The aqueous phase was extracted by CH_2Cl_2 and dried over $MgSO_4$, filtered and the solvent was removed. After purification by flash chromatography over silica gel using CH_2Cl_2:EtOH = 15:1 as eluant, compound **3** (*N*-(3,5-didodecyloxybenzyl)ethane-1,2-diamine) was obtained as a brown solid (denoted DA12 after its dodecyl tails). In the same manner, DA-lipids with hexyl, octyl, nonyl, decyl, dodecyl, pentadecyl, and octadecyl tails were synthesized and denoted DA6, DA8, DA9, DA10, DA12, DA15, and DA18. ^{1}H NMR (500 MHz, $CDCl_3$): δ 6.47 (2H, s, ArH), 6.39 (1H, s, ArH), 5.30 (1H, br s, NH), 3.88 (4H, t, $J =$ 6.5 Hz, 2 × OCH_2 and 2H, s, $CH_2CH_2NH_2$), 3.14 (2H, s, $NHCH_2CH_2$), 3.05 (2H, s, CH_2NH_2), 1.73 (4H, q, $J = 7.2$ Hz, 2 × OCH_2CH_2), 1.42–1.39 (4H, m, 2 × $OCH_2CH_2CH_2$), 1.29–

1.25 (44H, m, 2 × $C_{13}H_{27}$), 0.88 (6H, t, $J = 7.0$ Hz, 2 × CH_3).

pDNA Amplification. Plasmid DNA coding pGL3 (bp = 5256, where bp is the number of base pair) was amplified with *E. coli* competent cells and purified by using a QIAGEN HiSpeed Plasmid Maxi kit.

Preparation of Cationic Assemblies Formed from the Synthetic Lipids and Lipoplex. The cationic assemblies and lipoplex solutions were prepared as follows: A DA-lipid chloroform solution was poured into a 1 mL vial and dried in vacuo for 1 h, then an aqueous solution of an appropriate amount of NaCl was added to the vial to hydrate the lipid, the solution was then sonicated for 10 min with a UH-50 (SMT Co., Japan). The lipoplexes made from DA-lipid/DNA were prepared by mixing the DA lipid solution with an appropriate amount of sonicated salmon sperm DNA (the average number of base pair: bp was 3000) or a plasmid DNA (pGL3, bp = 5256) solution. Most experiments were carried out using plasmid DNA except calorimetry because it is homogeneous in size and data were less noisy. The DA-lipid/DNA mixing ratio was expressed in terms of the nitrogen to phosphate molar ratio: N/P. Here, it should be noted that the composition of the DA-lipid/DNA lipoplex is not always equal to N/P ratio because since free DNA or/and free lipid may exist in the mixture.

ANS Fluorescence Studies. The fluorescence probe 8-anilino-1-naphthalenesulfonic acid (ANS) was purchased from TCI and used without further purification. All solutions were prepared by diluting a stock solution (5 mM of DA, and in the case of the lipoplex 1.0 mg mL^{-1} of pDNA was added to adjust N/P = 6.6) with distilled water containing 50 mM NaCl. The concentration of ANS was fixed at 2.0×10^{-5} M. The fluorescence measurements were carried out with a fluorescence spectrophotometer (Hitachi F-4500), by exciting at 385 nm and recording the emission spectrum in the range 400–700 nm. The scan speed and the slit widths were 260 nm min^{-1} and 5.0 nm, respectively. From a plot of intensity vs. the lipid concentration, the critical micelle (CMC) and aggregation (CAC) concentrations were determined for the lipid and lipoplex solutions, respectively. CAC is defined as the point at which the polymer and surfactant start to form aggregates, in our case, at which DNA and DA form the ion-pair complex. The Gibbs free energy of surfactant aggregation can be calculated by the equation $\Delta G_{CAC} = -RT \ln \mathrm{CAC}$, according to Zhu et al.,[19] where R and T are the gas constant and temperature.

Synchrotron Small-Angle X-ray Scattering. SAXS measurements were carried out at BL40B2 SPring-8 with 0.71 and 0.54 m cameras equipped with a Rigaku imaging plate (30 × 30 cm, 3000 × 3000 pixels) employing an X-ray wavelength of 1.0 Å. The exposure time was 5 min and the relative X-ray intensity and the sample transmittance were determined with ion-chambers located in front of the sample and a photodiode behind. A bespoke chamber for SAXS measurements was constructed that enables a sample to be introduced in a vacuum and scattering measured from it as well as a vacuum-proof cell with a 0.20 mm quartz glass plate. Combining these two instruments, the data were then circularly averaged to produce one-dimensional (1-D) SAXS profiles of the scattered X-ray intensity [$I(q)$] versus the magnitude of the scattering vector (q), where q is related to the scattering angle θ and the wavelength of the X-ray λ through the relation of $q = 4\pi \sin\theta/\lambda$. SAXS experiments were performed at fixed concentrations of the DA lipid that were titrated against increasing pDNA concentrations.

Isothermal Titration Calorimetry. Heat flow during isothermal titration was measured with a VP-ITC MicroCal microcalorimeter (Northampton, MA). Titration data were processed with the software provided by the manufacturer. 50 μM bp (0.20 mg mL^{-1}) of the salmon DNA solution was maintained in the sample cell (1.401 mL) at 25 °C in 50 mM NaCl solution and the whole cell was stirred at 300 rpm. In each experiment 30 aliquots (7 μL each) of a stock solution of DA (2.0 mM) were automatically injected into a sample cell initially filled with DNA solution. Injections were 14 s in duration, and individual injections were programmed at intervals of 300 s. The injection intervals as well as the volume and the number of injections have been adjusted such that the binding is completed toward the end of the titration. After the peak area was integrated and the heats of dilution were subtracted, the thermogram for the binding was obtained.

Other Characterization. The ζ-potential and the average hydrodynamic radius (R_h) were measured with a Malvern Zetasizer nano (Malvern, U.K.) at rt. Transmission electron microscopy (TEM) was acquired using a JEOL TEM-3010 (accelerating voltage 200 kV). The sample was placed on 200-mesh carbon-coated copper (Cu) grids. The TEM grid was dried under reduced pressure for 12 h before observation.

Results and Discussion

N/P Dependence of ζ-Potential and R_h. It is important to know how the net surface charge and the size are changed when DNA is sequentially mixed with DA. The N/P dependence of the ζ-potential and the hydrodynamic radius (R_h) for DA12 and DA8 were investigated (Figure 2). For DA12 (triangles), when the complex had either a negative or positive ζ-potential in the range of N/P < 3 or N/P > 7, respectively, R_h was about

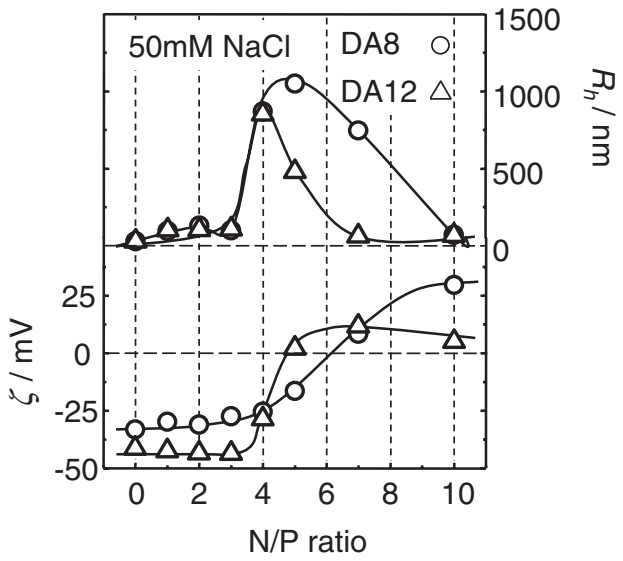

Figure 2. The N/P dependence of the ζ-potential and the hydrodynamic radius determined with DLS for DA8 and DA12.

100 nm or less. When we added pDNA at the isoelectric point around N/P = 5, R_h increased drastically, indicating that the complex underwent secondary aggregation. The isoelectric point of N/P = 5.0 indicates that about 40 mol % of DA12 are positively charged due to protonation of the diamine headgroup. Since the pK_a value of ethylenediamine in aqueous solutions is around 10[20], the relationship pH = pK_a + log([base]/[acid]) predicts that the DA12 head diamine is completely protonated at pH 7.0, which is in contradiction with the observed results. This discrepancy could be explained in a similar way to the Manning effect[21,22] in that clustered ion groups tend to be more neutralized by counter ion condensation to reduce electrostatic repulsion than free ions. The same phenomena was reported in the case of spermine and a spermine lipid (dioctadecylaminoglycyl spermine),[23] where the titration ended at [spermine]/[DNA] = 0.3 for spermine itself, while more spermine lipids were needed to reach the isoelectric point: [spermine lipid]/[DNA] = 0.5. When we used DA in DNA delivery, N/P was adjusted to 6.6 to obtain the highest transfection efficiency.[10] Therefore, we fixed N/P = 6.6 hereinafter unless otherwise noted. N/P dependences on the ζ-potential for DA18 were almost the same as DA12 (see the Supporting Information). The circular marks in Figure 2 show the N/P dependence of the ζ-potential and R_h for DA8. Comparing with those of DA12, the isoelectric point was similar with the DA12 system, around N/P = 5.0; however, there were relatively large particles in the positive potential side. Similar behavior was also observed for DA18, which may be related to the fact that DA18 showed less propensity to form complexes as opposed to DA12, as presented below.

Critical Micelle or Aggregation Concentration and Thermodynamics. The fluorescence intensity of ANS sensitively reflects the polarity of its environment and its intensity can be measured in dilute solutions such as less than 10^{-5} M of ANS. Therefore ANS is a useful probe for determination of CMC. The upper two panels of Figure 3 show examples of the ANS fluorescence intensity versus the lipid concentration (C_L) for DA8 and DA12 as well as their lipoplexes with the pDNA at N/P = 6.6. The obtained CMC and CAC values are summarized in Table S1 and plotted against N_C (alkyl tail length) in Figure 3. As presented in the lower panel in Figure 3, the CAC is around 10^{-2} mM for all N_C. The CMC is larger than CAC at $N_C = 5$ and 8 and decreases with an increase of N_C and seems to merge with the CAC at $N_C > 10$. CAC and CMC are observed in mixtures of polyelectrolytes and the oppositely charged ionic surfactants, and generally CAC is lower than CMC,[24–27] this relationship is also supported by theoretical considerations.[28] Although not all of the data are presented, the observed results, including Figure 3, are consistent with these general features for CAC and CMC. CMC of CTAB (hexadecyltrimethylammonium) and other cationic lipids such as CPC (hexadecylpyridinium chloride) and BAK12 (benzyldodecyldimethylammonium chloride) were determined to be 120 μM,[17] 60 μM (150 mM NaCl in phosphate buffered saline (PBS)),[19] and 1 mM (150 mM NaCl in PBS),[19] respectively. DOTAP ((2,3-dioleoylpropyl)trimethylammonium chloride), one of the most studied lipids in terms of lipoplex formation, has a CMC at 70 μM.[29] When a multi-amine group is attached as the headgroup such as

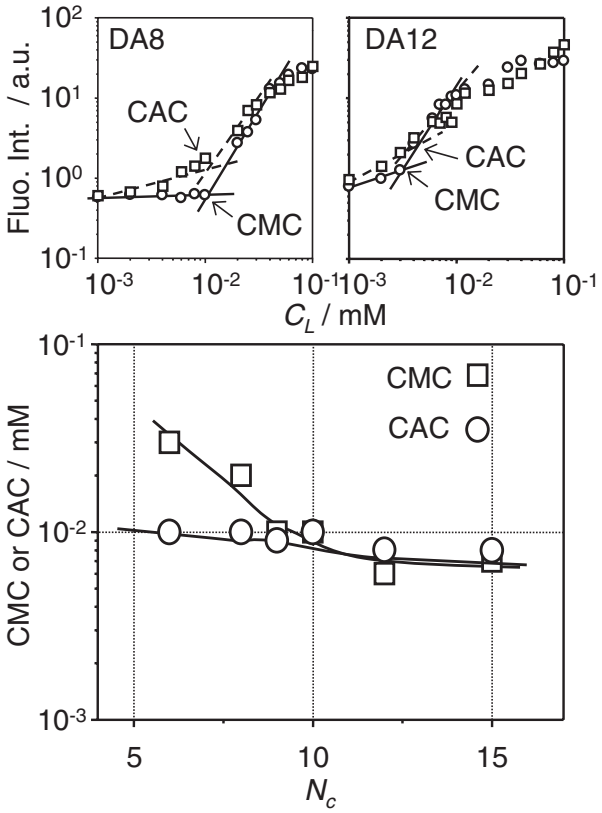

Figure 3. The DA concentration dependence of the ANS fluorescence intensity in DA8 (top left) and DA12 (top right), lipid (circles) and lipoplex (squares), and the DA alkyl tail length (N_C) dependence of the CMC and CAC (bottom) determined from intersections of the ANS fluorescence plots.

dioctadecylamidoglycyl spermine, the headgroup increases affinity with water and thus increases CMC. As presented in Table S1, CMC values for DA series are much lower than those of other compounds. This lower CMC can be attributed to the presence of the highly hydrophobic aromatic moiety of DA, which may form more attractive π–π stacking than the van der Waals interactions between alkyl chains in the vesicle. There are a few systematic studies of the CAC for cationic lipid/DNA systems. Zhu et al.[19] reported CAC for four compounds; 30 μM for CPC, 550 μM for BAK12, 46 μM for BAK14, and 550 μM for CTAC. From the isothermal titration curve for spermine lipid/DNA lipoplex, CAC can be estimated to be around 100 μM.[23] Comparing these values with those of DA-lipoplexes, it is clear that DA-lipoplexes show a considerably low CAC, ranging from about 10 μM. The thermograms of the titrations of the DA solutions into the DNA solutions are shown in the upper panel of Figure S1. The corresponding heat enthalpy change per mole of DA normalized with the DA concentration is presented in the lower panel of Figure S1. At 50 mM, a simple endothermic reaction was observed, indicating that the present system is driven by entropy gain. The thermogram showed drastic decrease with increasing DA concentration at N/P < 3, and finally the decrease seemed to finish at around N/P = 5.0 completely. This is in good agreement with the results obtained in the ζ-potential experi-

ment. The isothermal curve can be fit by a single site model and the obtained thermodynamic parameters are listed in Table S2. At 5 mM, the thermal response suggests that DA/DNA binding proceeds in a cooperative manner, the exothermal initial reaction leads to the subsequent endothermic reaction. Zhu and Evans[19] and Matulis et al.[17] observed a similar result and interpreted that there is no interaction below the CAC, but once DNA and lipid concentrations reach it, binding takes place. In our ITC experiments, we injected the 7 μL DA12 solution with $C_L = 2.0$ mM to a 1.401 mL DNA solution. Since the CMC for DA12 is 8 μM, the DA12 molecules in the ITC syringe had already formed the vesicle, and even at the first injection C_L in the sample cell should be beyond the CMC and CAC. Therefore, the thermodynamic parameters obtained here should be related to the interaction between the vesicle and DNA. With increasing salt concentration, the first exothermic binding mode disappeared and the second endothermic mode became dominate. This confirms that the first binding mode is due to electrostatic interactions between the anionic phosphate groups and cationic amine groups and the second one is due to the hydrophobic interactions that mainly cause the complexation. We analyzed the isothermal curve in terms of the two step sequential model.[30] Table S1 shows the ΔG_{CAC} values determined from $\Delta G_{CAC} = -RT \ln \mathrm{CAC}$.[19] The electrostatic contribution of monoamines is approximately estimated to be $-2.6\,\mathrm{kJ\,mol^{-1}}$,[17] which is almost equal to the observed first interaction. Referencing the ITC measurements for a series of alkylamines with long aliphatic chains, reveals the entropy gain for the aggregate formation due to the hydrophobic interaction between the alkyl chains is $T\Delta S = 5$–$10\,\mathrm{kJ\,mol^{-1}}$. ITC studies for DNA binding with CPC, BAK12,[19] and alkyl amines[17] showed that $T\Delta S = 5$–$20\,\mathrm{kJ\,mol^{-1}}$. These values are much smaller than those of the DA12 system, which reflect the fact that DA molecules consist of a highly hydrophobic aromatic moiety and the alkyl chains, although the nature of the interaction is completely different in the CAC and ITC experiments. At CAC, the DA molecules dissolved in water start to assemble triggered with the ion-pair formation with DNA, while ITC measured the DA-vesicle/DNA interactions. Nevertheless, the obtained free energies almost coincide with each other (see Table S1 and Table S2). This agreement suggests that the molecular origin of the entropy gain in both cases may be identical. It is difficult to uncover the origin of the large entropy gain upon complex formation. It is widely accepted that the major contribution in ITC comes from counter ion release, according to Wagner et al.[31] Additionally, dehydration may have also contributed to the positive change in entropy. With all these factors, one might suggest that the cationic group of DA lipid binds phosphate sites, while the DA hydrophobic group may have to lay down on the DNA. Therefore, the observed $T\Delta S$ is seemingly much larger than other cases. The large entropy gain and the agreement of ΔG from CAC and ITC suggest that the alkyl chain and aromatic moiety may also be involved in the complex formation.

Small-Angle X-ray Scattering from DA-Lipids. Figure 4 presents SAXS profiles from DA-lipids in 50 mM NaCl aqueous solution. We did not observe any Guinier region, suggesting that the scattering objects were too large to provide the overall size in the q range investigated. The intensity at low q seemed to follow the $I(q)$–$q^{-\alpha}$ relationship. Here, α is about 2.6 at DA6, it decreased with an increase of N_C and reached $\alpha = 2.0$ at DA15, except for DA18. DA18 showed an $\alpha = 2.5$, which may be a result of secondary aggregation. The presence of the aggregation was also supported by DLS for DA18 and thus we decided not to take account of the low q data for DA18. There was characteristic amplitude: Two minima at $q = 0.6$–1.0 and 3–$5\,\mathrm{nm^{-1}}$ and one maximum around $q = 1$–$2\,\mathrm{nm^{-1}}$, and their positions shifted toward lower q with an increase of N_C. For DA12 and DA15, a second maximum at $q = 3.5\,\mathrm{nm^{-1}}$ becomes appreciable, DA18 showed even a third maximum at $q = 6\,\mathrm{nm^{-1}}$. The presence of the higher maxima suggested that the local structure of these cationic assemblies are well defined and have a rather narrow distribution in size. One might suppose that we should be able to observe the $I(q)$–q^{-1} relationship at low q, as a characteristic relationship for the form factor of bilayer vesicles. This relationship is generally observed with neutron scattering in the range of $q \approx 10^{-3}\,\mathrm{nm^{-1}}$ or less.[32] To confirm vesicle formation, TEM observation for freeze-dried DA12 solution was performed, a typical image is presented in Figure 4B. The images seem to be torus shaped objects. We presume that these objects represent the vesicle made from DA12. To analyze SAXS from DA-lipid solutions, we supposed a bilayer vesicle model as presented in Figure 4C, where the bilayer consists of two shells made from the headgroups with a thickness of t_h and the core made of the alkyl tails with a thickness of t_c and the diameter of the vesicle is too large to give characteristic q dependence. The bilayer form factor for such a model can be expressed as below.[32–34]

$$I(q) = \frac{4\pi}{q^4}\left[(\rho_c - \rho_h)\sin\left(q\frac{t_c}{2}\right) + (\rho_h - \rho_s)\sin\left(q\frac{2t_h + t_c}{2}\right)\right]^2 \quad (1)$$

Here, ρ_c, ρ_s, and ρ_h are the electron densities for the hydrophobic core, solvent, and hydrophilic shell, respectively. By fitting the data with eq 1, we evaluated the best combination of ρ_h, t_h, and t_c, values so as to reproduce the data points under the condition of $\rho_s = 334\,\mathrm{e\,nm^{-3}}$ and $\rho_c = 277\,\mathrm{e\,nm^{-3}}$. Here, ρ_s was calculated from the NaCl concentrations and the electron density of water and ρ_c was assumed to take a value that had been reported for the alkyl domains for vesicle.[35] Since all DA molecules, regardless of the alkyl tail length, should have the same shell structure due to the identical headgroup, we decided to use the same values for t_h and ρ_h for all of the fitting. The most reliable values of ρ_s, t_h, and t_c were evaluated, the resultant values are summarized in Table 1. The best-fit curves are compared with the data as a solid line in Figure 4A. Agreement between the data and calculation is considerably good so as to conclude that DA forms a bilayer vesicle with the obtained structural parameters. From molecular modeling (MOPAC), a full stretch length of the alkyl chain of DA (L_t) was estimated and each value is listed in Table 1. At $N_C = 6$, $2L_t < t_c$, At $N_C = 8$, $2L_t \approx t_c$, and $N_C = 9$–18, $2L_t > t_c$. This fact indicates that when the tail is short, the methyl tail-tips do not enter the opposite side tail layer, yet with increasing tail length, they become intercalated with the opposite side or pack in a tilted tail-to-tail fashion.

Small-Angle X-ray Scattering from DA-Lipoplexes. Figure 5 presents the SAXS profiles when DNA was added

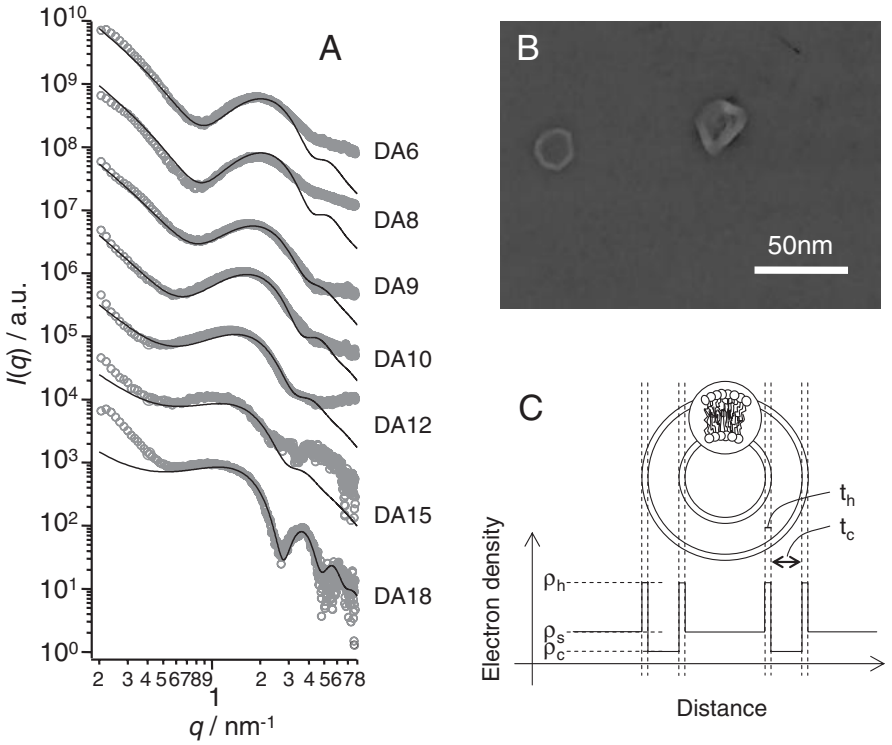

Figure 4. SAXS profiles from DA lipid (A), a typical TEM image for DA12 lipid solution after freeze-drying, depicting vesicles (B), and a schematic of the vesicle model used in the fitting (C).

Table 1. Structural Parameters Obtained from SAXS for the DA Vesicles and Lipoplexes

Sample code	t_c/nm[a),c)]	L_t/nm[b)]	Lamellar spacing (d)/nm at N/P = 3.0[c)]
DA6	1.80	0.75	4.82
DA8	1.82	1.01	4.87
DA9	1.92	1.14	5.06
DA10	2.13	1.25	5.16
DA12	2.35	1.51	5.44
DA15	2.63	1.89	6.17
DA18	2.91	2.28	6.41

a) When we analyzed the data with bilayer vesicle model, we found that the combination of $t_h = 0.30$ nm and $\rho_h = 575\,e\,nm^{-3}$ can give the best fitted curves for all DA samples. We fixed $\rho_c = 277\,e\,nm^{-3}$ and $\rho_s = 334\,e\,nm^{-3}$ based on the chemical compositions and densities. Therefore, only t_c is the adjustable parameter for the fitting. b) Full length of the alkyl tail calculated with a MOPAC program in Chem 3D. c) The experimental error range are $t_c = \pm 0.01$ nm, lamellar spacing (d) = ± 0.01 nm.

to DA (for DA6–DA18) at N/P = 3.0. All of the samples showed lamellar diffraction patterns, the lamellar distances (d) were determined from the peak positions, summarized in Table 1 and plotted against N_C in Figure 6, showing that the lamellar distance was increased with an increase of N_C. When the alkyl chain of the DA lipid is longer, attenuation of the second-order peak and broadening of the first-order peak indicate reduced regularity. Figures 7A and 7B present the N/P

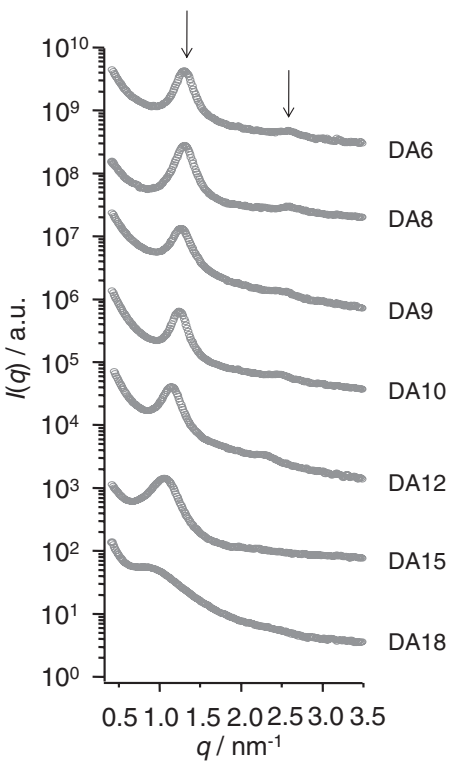

Figure 5. SAXS profiles from lipoplex solutions measured at SPring-8 BL40B2 with a 0.54 or 0.71 m camera at an X-ray wavelength of 1.0 Å: For the DA lipid/pDNA lipoplexes, N/P = 3.0.

dependence of SAXS for DA12. When we added DNA at N/P = 500 (in the molar ratio, DA12:base = 250:1), the form factor from the DA12 vesicle became completely invisible, and converted into diffraction from a lamella structure with the spacing $d = 5.02$ nm. Further addition of DNA increased the peak intensity in the range of N/P > 8. When DNA was added at N/P < 8, the spacing slightly increased and the peak intensity decreased upon addition of further DNA. Figure 8A plots d against N/P and Figure 8B plots the peak area against DNA concentration (where we chose DNA concentration instead of N/P ratio, because the peak intensity is proportional to the DNA concentration at N/P < 8 owing to the fixed lipid concentration.). The peak area increased proportionally with DNA concentration at N/P ≥ 8 (0.4 mM) and decreased at N/P < 8, except for N/P = 4. In Figure 7A, there was an upturn at low q region at N/P = 2–4. This upturn can be ascribed to aggregation. At N/P = 4, there was a large amount of precipitation in the cell because of the isoelectric point (Figure 2) and thus the concentration at the position of X-ray irradiation will be decreased, which explains the low peak intensity and thus deviation from the proportional line in Figure 8B. The N/P ratio dependences of d and the peak intensity in Figure 8 indicate that different mechanisms govern the formation of the lamellar at N/P > 8 and N/P < 8. Additionally, we found that d did not depend on the ionic strength (5–200 mM NaCl) and the difference between $d = 5.01$ and 5.44 nm at the two regions was confirmed to be beyond experimental error (the data are not presented). When we convert the ratio of N/P = 500 to the number of pDNA to DA, we find one pDNA to 1.31×10^6 DA molecules. Suppose the size of the vesicle is about 100 nm, one vesicle would consist of about $10^{4,5}$ DA molecules, which leads a ratio of one pDNA to approximately ten vesicles at N/P = 500. There are several other novel features observed in Figures 7 and 8 that have gone unnoticed in previous studies. The original vesicle scattering almost disappeared at N/P = 500, indicating that the addition of a very small amount of DNA drastically deformed the bilayer structure of the DA lipid. The size of pDNA with bp = 5256 is about 200–500 nm, which is about 2–5 times larger than one vesicle. The comparison in the ratio and size suggest that one pDNA can interact with all the vesicles at an

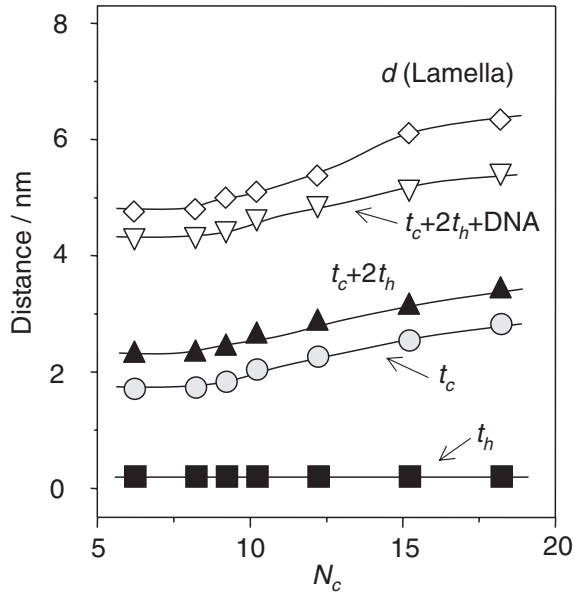

Figure 6. The alkyl tail length (N_C) dependence of the inner layer thickness (t_h), the total bilayer thickness ($2t_h + t_c$), the sum of $2t_h + t_c$ and the DNA diameter (2.0 nm), and the lamellar distance (d) at N/P = 3.0.

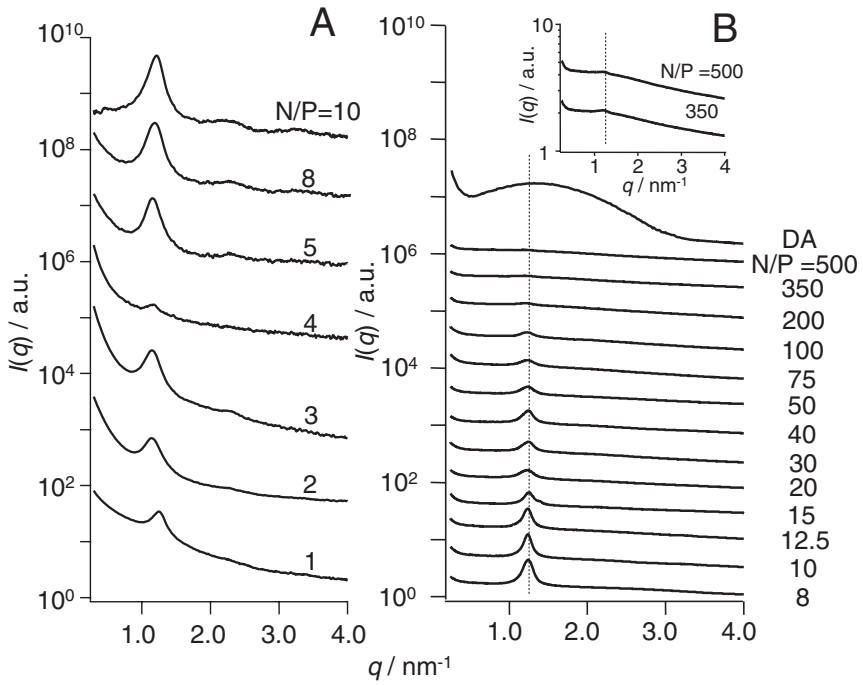

Figure 7. The N/P dependence (from 1 to 10) of the SAXS profiles (A) and the N/P dependence (from 8 to 500) for DA12/pDNA lipoplexes at a fixed DA12 concentration of 3.2 mM (B).

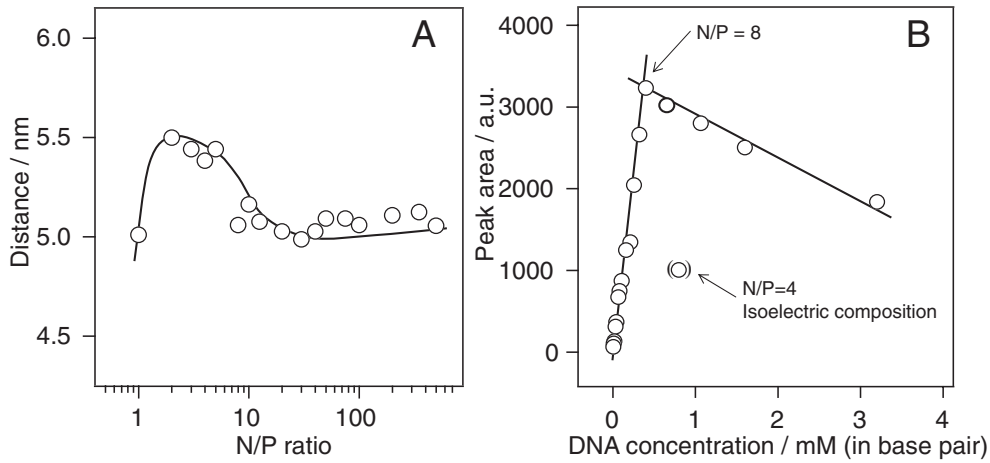

Figure 8. The N/P dependence of the lamellar distance (A) and the DNA concentration dependence of the first lamellar peak area (B). The area at N/P = 4 was reduced because of a decreased solution concentration due to precipitation at the isoelectric point.

N/P = 500. Once pDNA interacts with one vesicle, this event induces the entire vesicle to change its cross sectional structure. Furthermore, the first peak position did not shift upon further addition of DNA. If the number of the lamellar layers was less than 5, the peak position would shift to lower q (for example, two, three, and five layers satisfies the relation of $q_2/q_\infty = 0.917\cdots$, $q_3/q_\infty = 0.971\cdots$, and $q_5/q_\infty = 0.998\cdots$, respectively. q_n is the first peak position of the n layer lamellar). Therefore, the absence of shift in the peak position indicates that a multi-layer lamellar with at least 5 layers had been already formed at N/P = 500. Second, the peak intensity increasing proportionally to the DNA concentration implies that the formation of the lamellar proceeds in a stoichiometric manner and stoichiometric balance is achieved at one phosphate anion to four DA12 molecules (because the intensity reached the maximum at N/P = 8.0). This composition is different from the isoelectric point.

Vesicle to Lamellar Transition. Lamellar formation upon DNA/lipid interactions is well reported[3–5,36–42] and has attracted enormous interest since this phenomenon is related to DNA condensation and thus important in understanding the transfection efficiency of lipoplexes. Safinya et al. were the first to propose a structural model of the lamellar and their model has been widely used to analyze the lipoplex lamellar.[4] According to them, DNA molecules are confined to the two-dimensional cationic surface of the lamellar and sandwiched between the lipid bilayers (denoted $L_\alpha{}^C$ or DNA-sandwich model). On the other hand, Matulis et al.[17] and Marty et al.[8] showed that the presence of hydrophobic interaction via lipid aliphatic tails and hydrophobic region in DNA. According to their model, once DNA is coated with hydrophobic groups, the DNA/lipid complex could be transported into hydrophobic domain (denoted DNA-inclusion model). As presented in Figure 8, the lamellar peak (spacing = 5.01 nm) intensity increased proportionally to the DNA concentration at N/P ≥ 8 (0.4 mM). In the range of N/P < 8, the spacing increased to 5.5 nm and the intensity decreased with increasing DNA concentration. These different features for N/P ≥ 8 and N/P < 8 suggest that the lamellar supramolecular structures differ according to the composition. At N/P < 8 (including the negative side in Figure 2), all of the added DA molecules should be interacting with DNA. The only suitable model to explain the lamellar formation in this case is the sandwich model. This can be confirmed when $t_c + 2t_h +$ the diameter of DNA (2.0 nm) is plotted as a function of N_C as shown in Figure 5. The values of $t_c + 2t_h +$ DNA are smaller than that of d at N/P = 3.0, the difference between them is approximately 0.6 nm at $N_C = 6$ and increases to approximately 1.1 nm at $N_C = 18$. The model for the region of N/P > 8 seems to be rather difficult to establish. When we added a small amount of DNA to DA-vesicle solutions, we also observed lamellar formation. This can be explained by either the sandwich or inclusion model, while it is difficult to draw a definitive conclusion only from the present SAXS data.

Conclusion

We synthesized a series of aromatic diamine lipids (DA) with alkyl tail lengths from C6 to C18 and explored the DA/DNA complexes as a function of N/P with DLS, SAXS, and ITC. The following facts are clarified: (1) The isoelectric point was achieved at N/P = 5.0, (2) the CMC and CAC were determined to be around 10 μM, which is very small compared with other cationic lipids, (3) SAXS profiles from the DA lipids were reproduced with a monolayer vesicle model, (4) SAXS profiles from the lipoplexes showed that lamellar were formed upon complexation, (5) When the N/P dependence of SAXS were measured, characteristic vesicle scattering disappeared even at N/P = 500 and the lamellar peak area reached a maximum at N/P = 8, (6) the lamellar spacing was about 5.5 nm at N/P < 8, while it was about 5.0 nm at N/P > 8, (7) ITC showed the DA/DNA complexation was driven by entropy. These results at N/P < 8 can be rationalized by assuming the sandwich model. However, two possible models [sandwich or inclusion model] can be considered for the range of N/P > 8.

This work is finically supported by the JST CREST program. All SAXS measurements were carried out at SPring-8 BL40B2 (No. 2008B0012). The Royal Society, U.K. (International Joint Project) are thanked for support.

Supporting Information

ITC for DA12, DLS and ζ-potential for DA18, Tables for CMC, CAC data. This material is available free of charge on the web at http://www.csj.jp/journals/bcsj/.

References

1 L. Huang, H. Mien-Chie, E. Wanger, *Nonviral Vectors for Gene Therapy*, Academic Press, San Diego, **1999**.

2 P. L. Felgner, T. R. Gadek, M. Holm, R. Roman, H. W. Chan, M. Wenz, J. P. Northrop, G. M. Ringold, M. Danielsen, *Proc. Natl. Acad. Sci. U.S.A.* **1987**, *84*, 7413.

3 I. Koltover, T. Salditt, J. O. Rädler, C. R. Safinya, *Science* **1998**, *281*, 78.

4 J. O. Rädler, I. Koltover, T. Salditt, C. R. Safinya, *Science* **1997**, *275*, 810.

5 C. R. Safinya, *Curr. Opin. Struct. Biol.* **2001**, *11*, 440.

6 A. Zidovska, H. M. Evans, K. K. Ewert, J. Quispe, B. Carragher, C. S. Potter, C. R. Safinya, *J. Phys. Chem. B* **2009**, *113*, 3694.

7 K. Ewert, N. L. Slack, A. Ahmad, H. M. Evans, A. J. Lin, C. E. Samuel, C. R. Safinya, *Curr. Med. Chem.* **2004**, *11*, 133.

8 R. Marty, C. N. N'Soukpoé-Kossi, D. Charbonneau, C. M. Weinert, L. Kreplak, H.-A. Tajmir-Riahi, *Nucleic Acids Res.* **2009**, *37*, 849.

9 K. Koiwai, K. Tokuhisa, R. Karinaga, Y. Kudo, S. Kusuki, Y. Takeda, K. Sakurai, *Bioconjugate Chem.* **2005**, *16*, 1349.

10 K. Sakurai, S. Kusuki, E. Hamada, Y. Takeda, Jpn. Kokai Tokkyo Koho 2008-143844, **2008**.

11 K. Shimizu, M. Isozaki, K. Koiwai, U.S. Patent 6228391, **2001**.

12 K. Kawahara, A. Sekiguchi, E. Kiyoki, T. Ueda, K. Shimamura, Y. Kurosaki, S. Miyaoka, H. Okabe, M. Miyajima, J. Kimura, *Chem. Pharm. Bull.* **2003**, *51*, 336.

13 M. Sakuragi, S. Kusuki, E. Hamada, H. Masunaga, H. Ogawa, I. Akiba, K. Sakurai, *J. Phys.: Conf. Ser.* **2009**, *184*, 012008.

14 R. Koynova, R. C. MacDonald, *Biochim. Biophys. Acta* **2007**, *1768*, 2373.

15 R. Koynova, Y. S. Tarahovsky, L. Wang, R. C. MacDonald, *Biochim. Biophys. Acta* **2007**, *1768*, 375.

16 R. Koynova, B. Tenchov, L. Wang, R. C. Macdonald, *Mol. Pharmacol.* **2009**, *6*, 951.

17 D. Matulis, I. Rouzina, V. A. Bloomfield, *J. Am. Chem. Soc.* **2002**, *124*, 7331.

18 C. H. Spink, J. B. Chaires, *J. Am. Chem. Soc.* **1997**, *119*, 10920.

19 D.-M. Zhu, R. K. Evans, *Langmuir* **2006**, *22*, 3735.

20 V. S. Bryantsev, M. S. Diallo, W. A. Goddard, III, *J. Phys. Chem. A* **2007**, *111*, 4422.

21 G. S. Manning, *J. Chem. Phys.* **1969**, *51*, 924.

22 G. S. Manning, *J. Phys. Chem. B* **2007**, *111*, 8554.

23 M. M. Patel, T. J. Anchordoquy, *Biophys. J.* **2005**, *88*, 2089.

24 D. Y. Chu, J. K. Thomas, *J. Am. Chem. Soc.* **1986**, *108*, 6270.

25 P. Hansson, M. Almgren, *J. Phys. Chem.* **1995**, *99*, 16694.

26 P. Hansson, M. Almgren, *J. Phys. Chem.* **1996**, *100*, 9038.

27 M. Nichifor, M. Bastos, S. Lopes, A. Lopes, *J. Phys. Chem. B* **2008**, *112*, 15554.

28 H. Diamant, D. Andelman, *Macromolecules* **2000**, *33*, 8050.

29 J. Dalvi-Malhotra, L. Chen, *J. Phys. Chem. B* **2005**, *109*, 3873.

30 T. Wiseman, S. Williston, J. F. Brandts, L.-N. Lin, *Anal. Biochem.* **1989**, *179*, 131.

31 K. Wagner, D. Harries, S. May, V. Kahl, J. O. Rädler, A. Ben-Shaul, *Langmuir* **2000**, *16*, 303.

32 S. Ristori, J. Oberdisse, I. Grillo, A. Donati, O. Spalla, *Biophys. J.* **2005**, *88*, 535.

33 L. Cantù, M. Corti, E. Del Favero, M. Dubois, T. N. Zemb, *J. Phys. Chem. B* **1998**, *102*, 5737.

34 A. Salvati, S. Ristori, J. Oberdisse, O. Spalla, G. Ricciardi, D. Pietrangeli, M. Giustini, G. Martini, *J. Phys. Chem. B* **2007**, *111*, 10357.

35 T. Kawaguchi, T. Hamanaka, Y. Kito, H. Machida, *J. Phys. Chem.* **1991**, *95*, 3837.

36 K. K. Ewert, H. M. Evans, A. Zidovska, N. F. Bouxsein, A. Ahmad, C. R. Safinya, *J. Am. Chem. Soc.* **2006**, *128*, 3998.

37 T. Kawashima, A. Sasaki, S. Sasaki, *Biomacromolecules* **2006**, *7*, 1942.

38 I. Koltover, T. Salditt, C. R. Safinya, *Biophys. J.* **1999**, *77*, 915.

39 I. Koltover, K. Wagner, C. R. Safinya, *Proc. Natl. Acad. Sci. U.S.A.* **2000**, *97*, 14046.

40 R. Koynova, L. Wang, R. C. MacDonald, *Proc. Natl. Acad. Sci. U.S.A.* **2006**, *103*, 14373.

41 C. R. Safinya, E. B. Sirota, R. J. Plano, *Phys. Rev. Lett.* **1991**, *66*, 1986.

42 S. Zhou, D. Liang, C. Burger, F. Yeh, B. Chu, *Biomacromolecules* **2004**, *5*, 1256.